Imposing the boundary conditions in the LBIE/RBF method: a simplified approach

E. H. Ooi & V. Popov
Environmental and Fluid Mechanics, Wessex Institute of Technology, UK

Abstract

A simple approach for imposing the boundary conditions in the local boundary integral equation (LBIE) method is proposed. The proposed approach maintains the weak formulation on the boundary by enforcing the integral equation derived from the Green's second identity and the fundamental solution of the Laplace equation. Unlike in the LBIE, the subdomains at the boundary in the proposed method preserve their circular shapes, such that difficulties associated with the evaluation of near-singular and singular integrals and the determination of intersection between the global and local boundaries can be avoided. The proposed approach is compared with the conventional LBIE by solving the convection-diffusion equation. The unknown field variables were approximated with the RBF approximations. Numerical results showed that the proposed method, despite its simplicity, yielded results of comparable accuracy with the LBIE when third order RBF was used.
Keywords: local boundary integral equation, weak formulation, radial basis functions, meshless methods, companion solution.

1 Introduction

The local boundary integral equation (LBIE) method is a meshless method developed by Zhu *et al.* [1] that combines the advantages of several numerical methods including the Galerkin finite element method, the boundary element method and the element-free Galerkin method. Implementation of the LBIE involves the distribution of collocation nodes over the boundary and interior of the solution domain, whereby a circular (spherical in 3D) subdomain centred on each node is generated. In each subdomain, the integral equation derived from the governing equation holds. The LBIE introduces the concept of

WIT Transactions on Modelling and Simulation, Vol 53,
www.witpress.com, ISSN 1743-3533 (on-line)
doi:10.2495/BE120061

a companion solution such that the single layer integral is eliminated from the local integral equations. The unknown field variables are approximated using the moving least squares (MLS) approximation, although other interpolation schemes such as the radial basis function (RBF) approximation have been implemented successfully. In particular, the LBIE employing the RBF approximations has been known as the LBIE/RBF [2].

When the collocation node is at the global boundary, the subdomain in the LBIE is defined by the overlapping part between the circular subdomain and the solution domain, while the local boundary is defined by part of the circular boundary that is inside the solution domain and part of the global boundary where the circular boundary intersects, see Figure 1. In this case, the companion solution does not vanish on part of the global boundary. Consequently, there is a need to evaluate the single and double layer integrals when imposing the boundary conditions for the nodes at the global boundary. This involves the calculations of near-singular and singular integrals, which are mathematically more challenging to solve. The problem is further compounded by the need to determine the intersection between the global and local boundaries, which is a cumbersome task especially in 3D problems. Although these issues may be avoided by using the MLS collocation scheme to impose the boundary conditions, this approach abandons the weak formulation on the boundary and requires a highly accurate interpolation scheme to yield accurate numerical results.

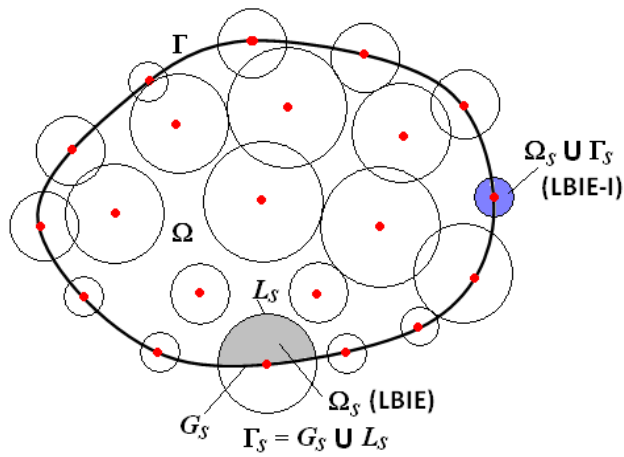

Figure 1: (Color online) Distribution of collocation nodes and their corresponding subdomains. Grey and blue represents subdomains on the global boundary for the LBIE and the LBIE-I, respectively.

A simple approach for imposing the boundary conditions in the LBIE, more specifically, the LBIE/RBF, is proposed here. The proposed method maintains the weak formulation by enforcing the integral equation derived using the fundamental solution and the Green's second identity on the boundary. The

subdomains for the nodes on the boundary preserve their circular shapes. Unknown field variables that are exterior to the solution domain are extrapolated using neighbouring nodes. Consequently, no near-singular and singular integrals are encountered, since the source point is always located at the centre of the subdomain. The daunting task of locating the intersection between the local and global boundaries can also be avoided. For nodes at the interior, the approach is the same as in the conventional LBIE. For simplicity, the LBIE adopting the proposed approach for imposing the boundary condition is hereafter referred to as the LBIE-I.

The mathematical derivations of the LBIE and the LBIE-I are presented in the next section. Section 3 outlines the RBF approximation scheme used in this study. The numerical implementation of the LBIE and the LBIE-I are given in Section 4. Comparisons between the LBIE and the LBIE-I are presented in Section 5 and the conclusions are given in Section 6.

2 Mathematical formulations

2.1 Problem definition

Consider the domain Ω bounded by the close curve Γ defined in the two-dimensional Cartesian coordinate system. The equation governing the steady-state potential distribution in $\Omega \cup \Gamma$ is given by

$$\nabla^2 u(r) = b, \quad \text{for } r \in \Omega \cup \Gamma, \tag{1}$$

where $r = (x_1, x_2)$ are the coordinates of the field point, u is the potential and b is the source term, where $b \equiv b(r, u, \partial u/\partial x_i)$. To complete the problem definition, (1) is subjected to the following boundary conditions:

$$\begin{aligned} u(r) &= u_o, \quad \text{on } \Gamma_1, \\ \frac{\partial u(r)}{\partial n} &= q_o, \quad \text{on } \Gamma_2, \end{aligned} \tag{2}$$

where u_o and q_o are suitably prescribed functions and Γ_1 and Γ_2 are two non-intersecting parts of Γ such that $\Gamma = \Gamma_1 \cup \Gamma_2$.

2.2 The local boundary integral equation

To carry out the LBIE, a series of N_t nodes are distributed over $\Omega \cup \Gamma$. A circular subdomain, Ω_s centred on each node is generated, see Figure 1. For nodes at the global boundary, the subdomain is taken as the overlapping part between the circular subdomain and the solution domain (see grey region in Figure 1).

Using the Green's second identity and the fundamental solution of the Laplace equation, the integral equation of (1) defined over the subdomain Ω_s can be derived, which is given by

$$u(r)\big|_{r=\xi} = \int_{\Gamma_s} u(r)\frac{\partial \Phi(r;\xi)}{\partial n} - \Phi(r;\xi)\frac{\partial u(r)}{\partial n}\mathrm{d}\Gamma + \iint_{\Omega_s} b\cdot\Phi(r;\xi)\mathrm{d}\Omega, \tag{3}$$

where Γ_s is the local boundary of the subdomain Ω_s, ξ is the source point and $\Phi(r;\xi)$ is the fundamental solution of the Laplace equation. By introducing the companion solution [1] for subdomains which do not have contact with the global boundary, (3) reduces to

$$u(r)\big|_{r=\xi} = \int_{\Gamma_s} u(r)\frac{\partial \Phi^*(r;\xi)}{\partial n}\mathrm{d}\Gamma + \iint_{\Omega_s} b\cdot\Phi^*(r;\xi)\mathrm{d}\Omega, \tag{4}$$

for ξ at the interior. When ξ is at the boundary the following equation is used

$$\begin{aligned}\lambda(r)u(r)\big|_{r=\xi} = &\int_{\Gamma_s} u(r)\frac{\partial \Phi^*(r;\xi)}{\partial n}\mathrm{d}\Gamma + \int_{L_s} u(r)\frac{\partial \Phi^*(r;\xi)}{\partial n}\mathrm{d}\Gamma \\ &- \int_{G_s} u(r)\frac{\partial \Phi^*(r;\xi)}{\partial n}\mathrm{d}\Gamma + \iint_{\Omega_s} b\cdot\Phi^*(r;\xi)\mathrm{d}\Omega,\end{aligned} \tag{5}$$

where G_s and L_s are the global and local sections of the local boundary Γ_s, see Figure 1, λ is a geometric coefficient such that $\lambda = \theta/2\pi$, where θ is the internal angle at the boundary and $\Phi^*(r;\xi)$ is the modified test function given by [1]

$$\Phi^*(r;\xi) = \frac{1}{2\pi}\log\left(\frac{\Re(r;\xi)}{\Re_s}\right), \tag{6}$$

where $\Re$ is the Euclidean distance between the field point r and the source point ξ and $\Re_s$ is the radius of the subdomain Ω_s. For more details on the derivation of the LBIE, one may refer to the works of Zhu *et al*. [1].

2.3 The local boundary integral equation-I

The formulation of the LBIE-I is the same as in the LBIE when the collocation node is at the interior, i.e. (4) is used. For the nodes at the global boundary, the following equation, which is obtained by differentiating (3) with respect to the source point, is used:

$$\begin{aligned}\left.\frac{\partial u(r)}{\partial x_i}\right|_{r=\xi} = &\int_{\Gamma_s} u(r)\frac{\partial^2 \Phi(r;\xi)}{\partial x_i \partial n} - n_j\frac{\partial u(r)}{\partial x_j}\frac{\partial \Phi(r;\xi)}{\partial x_i}\mathrm{d}\Gamma \\ &+ \iint_{\Omega_s} b\cdot\Phi(r;\xi)\mathrm{d}\Omega,\end{aligned} \tag{7}$$

where n_j are the components of the outward unit normal vector. The boundary integral on the right hand side of (7) is carried out over the complete circular boundary of the subdomain (see blue region in Figure 1).

3 The radial basis function approximation

In this study, the unknown field variables in (4), (5) and (7) are approximated in terms of the neighbouring nodes by using the RBF approximations, i.e.

$$u(r) = \sum_{k=1}^{N_a} \alpha^{(k)} f(r; r^{(k)}), \tag{8}$$

where N_a is the number of points used in the RBF approximation, $f(r;r^{(k)})$ is the RBF and $\alpha^{(k)}$ are unknown coefficients, which may be expressed as

$$\alpha^{(k)} \approx \sum_{n=1}^{N_a} W^{(kn)} u_n, \quad \text{for } k = 1, 2, \ldots, N_a - 1, N_a, \tag{9}$$

where the coefficients $W^{(kn)}$ are explicitly given by

$$\sum_{n=1}^{N_a} W_{kn} f(r^{(n)}; r^{(p)}) = \begin{cases} 1, \text{if } p = k \\ 0, \text{if } p \neq k \end{cases}, \quad \text{for } p, k = 1, 2, \ldots, N_a - 1, N_a. \tag{10}$$

Substituting (9) into (8) yields

$$u(r) \approx \sum_{n=1}^{N_a} u_n \sum_{k=1}^{N_a} W^{(kn)} f(r; r^{(k)}). \tag{11}$$

where u_n is the value of u at the n^{th} approximation point. In the LBIE-I, the unknown variables $\partial u(r)/\partial x_j$ in (7) are expressed in terms of u by differentiating (11). This leads to

$$\frac{\partial u(r)}{\partial x_j} \approx \sum_{n=1}^{N_a} u_n \sum_{k=1}^{N_a} W^{(kn)} \frac{\partial f(r; r^{(k)})}{\partial x_j}. \tag{12}$$

The choice of the RBF used has a strong influence on the accuracy of the numerical solutions. One of the most commonly used RBF in variables approximation is the polyharmonic spline, which in 2D, has two different forms, i.e.

$$f(r; r^{(k)}) = \begin{cases} \Re^{2n-1}(r; r^{(k)}) \\ \Re^{2n} \log(\Re(r; r^{(k)})) \end{cases}, \quad \text{for } n = 1, 2, 3, \ldots \tag{13}$$

The polyharmonic spline in (13) is usually augmented with global polynomials of the form

$$p_n(r) = a_o + a_1 x + a_2 y + a_3 x^2 + a_4 xy + a_5 y^2 + \ldots, \tag{14}$$

where a_i (for i = 0, 1, 2, ….) are unknown coefficients to be determined.

The order of the polynomial used in the augmentation depends on the order of the RBF used. For instance, if a second order RBF is used (n = 2 in (13)), then the second order polynomial, i.e. up to six terms in (14) should be used. The polynomial augmentation is important to ensure convergence of the RBF approximation [3].

4 Numerical implementation

In the LBIE, (3) is used in the assembly of the system of equations when the collocation node is at the interior. Substituting (11) into (3) leads to

$$u(r)\big|_{r=\xi} = \sum_{n=1}^{N_a} u_n \sum_{k=1}^{N_a} W^{(kn)} H_k + \iint_{\Omega_s} b \cdot \Phi^*(r;\xi)\mathrm{d}\Omega, \tag{15}$$

where

$$H_k = \int_{\Gamma_s} f(r;r^{(k)}) \frac{\partial \Phi^*(r;\xi)}{\partial n}\mathrm{d}\Gamma. \tag{16}$$

When the collocation node is at the boundary where the Dirichlet condition is specified, no equation is enforced here since the value of potential is already known. When the collocation node is at the boundary where the Neumann condition is specified, (4) is used, where upon substituting for (11), yields

$$\lambda(r)u(r)\big|_{r=\xi} = \sum_{n=1}^{N_a} u_n \sum_{k=1}^{N_a} W^{(kn)}[F_{1k} + F_{2k}] - F_{3k} + \iint_{\Omega_s} b \cdot \Phi^*(r;\xi)\mathrm{d}\Omega, \tag{17}$$

where

$$\begin{aligned} F_{1k} &= \int_{L_s} f(r;r^{(k)}) \frac{\partial \Phi^*(r;\xi)}{\partial n}\mathrm{d}\Gamma, \\ F_{2k} &= \int_{G_s} f(r;r^{(k)}) \frac{\partial \Phi^*(r;\xi)}{\partial n}\mathrm{d}\Gamma, \\ F_{3k} &= \int_{G_s} \Phi^*(r;\xi) q_o \mathrm{d}\Gamma. \end{aligned} \tag{18}$$

In the LBIE-I, the equation used when the node is at the interior is the same as in the LBIE, i.e. (15) is used. Likewise, at the boundary where the Dirichlet condition is specified, no equation is used. When the collocation node is at the boundary where the Neumann condition is specified, (7) is used, where upon substituting (11) and (12), yields

$$q_o(\xi)=\sum_{n=1}^{N_a}u_n\sum_{k=1}^{N_a}W^{(kn)}[G_{1k}-G_{2k}-G_{3k}]+\iint_{\Omega_s}b\cdot n_i(\xi)\cdot\frac{\partial\Phi(r;\xi)}{\partial x_i}\,\mathrm{d}\Omega, \tag{19}$$

where

$$\begin{aligned}
G_{1k}&=\int_{\Gamma_s}f(r;r^{(k)})\cdot n_i(\xi)\cdot\frac{\partial^2\Phi(r;\xi)}{\partial x_i\partial n}\,\mathrm{d}\Gamma,\\
G_{2k}&=\int_{\Gamma_s}n_x(r)\cdot\frac{\partial f(r;r^{(k)})}{\partial x}\cdot n_i(\xi)\cdot\frac{\partial\Phi(r;\xi)}{\partial x_i}\,\mathrm{d}\Gamma,\\
G_{3k}&=\int_{\Gamma_s}n_y(r)\cdot\frac{\partial f(r;r^{(k)})}{\partial y}\cdot n_i(\xi)\cdot\frac{\partial\Phi(r;\xi)}{\partial x_i}\,\mathrm{d}\Gamma,
\end{aligned} \tag{20}$$

and $n_i(\xi)\cdot(\partial/\partial x_i)=n_x(\xi)\cdot(\partial/\partial x)+n_y(\xi)\cdot(\partial/\partial y)$.

5 Numerical example

In this section, the LBIE-I is compared with the LBIE by solving the convection-diffusion equation:

$$\nabla^2u(r)=V_x(r)\frac{\partial u(r)}{\partial x}+ku(r), \tag{21}$$

where k is the reaction rate and $V_x(r)$ is the velocity field given by

$$V_x(r)=\ln\left(\frac{U_1}{U_o}\right)+k\left(x-\frac{1}{2}\right), \tag{22}$$

where U_1 and U_o are suitably prescribed functions. The solution domain was chosen to be $0\le x\le L$ and $-W\le y\le W$. The following boundary conditions were applied:

$$u(0,y)=U_o,\quad u(L,y)=U_1,\quad \frac{\partial u(x,\pm W)}{\partial n}=0. \tag{23}$$

The exact solution is given by $u(r)=U_o\exp\{0.5kx^2+(x/L)[\ln(U_1/U_o)]-0.5kLx\}$.

The values of W, L, U_1 and U_o were chosen to be 0.25, 1, 10 and 4, respectively. Two different values of k were considered, i.e. 10 and 40. Numerical simulations were carried out using N_a = 25 points in the RBF approximations. The integrals over the local boundary (see (15) to (20)) and the domain integrals are evaluated numerically using the Gaussian quadrature with 20 and 400 Gaussian points, respectively. The integrals over the global boundary (see 2nd and 3rd lines in (18)) were evaluated analytically based on the formulae reported in Ang [4]. The LBIE and the LBIE-I were tested using two different

RBFs, i.e. $\Re^4\log(\Re)$ augmented with the second order global polynomial and $\Re^6\log(\Re)$ augmented with the third order global polynomial.

Results from the numerical simulations showed that the LBIE produced more accurate results than the LBIE-I in the calculations of u when the RBF $\Re^4\log(\Re)$ was used; although the differences in the L_2 norm error between the LBIE and the LBIE-I decreased with increasing k (results not presented here). Negligible differences in the L_2 norm errors were observed in the calculations of $\partial u/\partial x$.

Figure 2 plots the L_2 norm errors of u and $\partial u/\partial x$ against the total number of nodes for the cases when the RBF $\Re^6\log(\Re)$ was used. The L_2 norm error decreased with increasing number of nodes in both the LBIE and the LBIE-I; suggesting convergence in the numerical schemes. The LBIE-I was found to produce more accurate results than the LBIE as the number of nodes increased for the case when $k = 10$. For the case when $k = 40$, the LBIE was more accurate than the LBIE-I when the number of nodes used was less than approximately 6000. As the number of nodes increased, the accuracy of the LBIE and the LBIE-I became comparable.

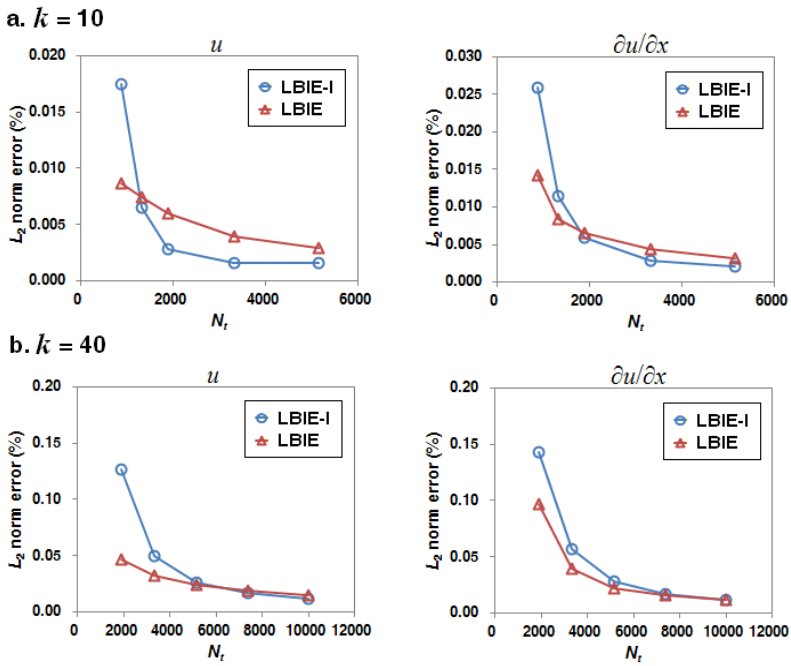

Figure 2: Plots of the L_2 norm errors of u and $\partial u/\partial x$ against the total number of nodes used obtained using the RBF $\Re^6\log(\Re)$ for: (a) $k = 10$ and (b) $k = 40$.

Figure 3 plots the spatial distribution of the percentage errors for u and $\partial u/\partial x$. The LBIE-I produced higher percentage errors along the boundary while the maximum percentage error of the LBIE was concentrated at the centre of the domain.

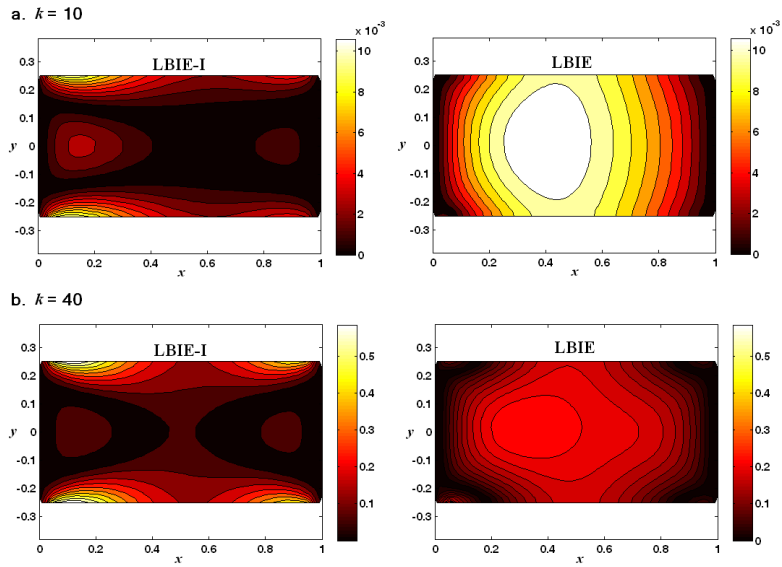

Figure 3: Distribution of the percentage error of u (%) in test problem 4 for: (a) $k = 10$ and (b) $k = 40$, obtained using the RBF $\Re^6\log(\Re)$ and 1891 collocation nodes.

Table 1 summarizes the total CPU time of the LBIE and the LBIE-I. The total CPU time represents the sum of the times needed to evaluate the boundary and domain integrals (see (15) to (20)), to assemble the system of linear algebraic equations and to solve the system matrix. The total CPU time includes also the time needed to calculate $\partial u/\partial x$ by using (7) during post-processing. The CPU time of the LBIE-I is shorter than the LBIE although the differences were not significant.

Table 1: Total CPU time of the LBIE and the LBIE-I.

Number of nodes	Total CPU time (s)	
	LBIE-I	LBIE
861	8.81	9.73
1326	14.08	16.14
1891	20.27	22.53
3321	37.22	40.94
5151	61.33	66.47
7381	96.16	102.17

6 Conclusions

A simplified approach for imposing the boundary conditions in the LBIE has been proposed. The proposed method maintains the weak formulation on the boundary by enforcing the integral equation derived from the Green's second identity and the fundamental solution of the Laplace equation.

The LBIE-I was compared with the LBIE by solving the convection-diffusion equation. When the lower order RBF ($\Re^4\log(\Re)$) was used, the accuracy of the LBIE-I was lower compared to the one of the LBIE. However, when the higher order RBF ($\Re^6\log(\Re)$) was used, the LBIE-I was found to be of comparable accuracy to the LBIE. This may be explained by the differentiation of the RBF approximation used when approximating the potential gradient in the integral equation in the LBIE-I. Differentiation reduces the order of the RBF approximations by one. This leads to the decrease in the accuracy of the approximations on the boundary. Consequently, if the RBF is not carefully chosen, the numerical results obtained, especially along the boundaries can be less accurate. Computations with the LBIE-I took slightly shorter CPU time compared to the LBIE.

The LBIE-I offers an appealing alternative for imposing the boundary conditions. Unlike the LBIE, the subdomains at the global boundary in the proposed formulation preserve their circular shapes. Hence, the difficulty associated with the evaluation of near-singular and singular integrals can be avoided. Furthermore, since the intersections between the global and local boundaries are not required, extension of the method to 3D cases is straightforward.

References

[1] Zhu T, Zhang J.D. and Atluri S.N., A local boundary integral equation (LBIE) method in computational mechanics, and a meshless discretization approach, *Computational Mechanics*, 1998; 21:223–235.
[2] Sellountos E.J. and Sequeira A., An advanced meshless LBIE/RBF method for solving two-dimensional incompressible fluid flows, *Computational Mechanics*, 2008; 41:617–631.
[3] Cheng A.H.D., Particular solutions of Laplacian, Helmholtz-type, and polyharmonic operators involving higher order radial basis functions, *Engineering Analysis with Boundary Elements*, 2000; 24:531–538.
[4] Ang W.T., *A beginner's course in boundary element methods*, 2007, Universal Publishers, Boca Raton, Florida.